Soft Matter

PAPER

Phase behavior and microstructures in a mixture of anionic Gemini and cationic surfactants

Haiming Fan,*[ab] Bingcheng Li,[a] Yun Yan,[b] Jianbin Huang*[ab] and Wanli Kang[a]

We report in this work the phase behavior and microstructures in a mixture of an anionic Gemini surfactant, sodium dilauramino cystine (SDLC), and a conventional cationic surfactant, dodecyl trimethyl ammonium chloride (DTAC). Observation of the appearance shows that the phase behavior of the SDLC–DTAC mixed cationic surfactant system transforms from an isotropic homogeneous phase to an aqueous surfactant two-phase system (ASTP) and then to an anisotropic homogeneous phase with the continuous addition of DTAC. The corresponding aggregate microstructures are investigated by rheology, dynamic light scattering, transmission electron microscopy and polarization microscopy. It has been found that a wormlike micelle, in the isotropic homogeneous phase, occurs linear to the branch growth. The aggregate microstructures in the ASTP lower and upper phases are branched wormlike micelles and vesicles, respectively. The micelle transformed into a vesicle upon varying the phase volume percentage until a lamellar liquid crystal formed in the anisotropic homogeneous phase. The macroscopic phase behavior and microscopic aggregate structure are related to the understanding of the possible mechanisms for the above phenomena.

Introduction

It is well known that aqueous mixtures of anionic and cationic surfactants exhibit interesting interfacial properties and phase behavior, which mainly arise from electrostatic interactions between oppositely charged head groups.[1] One pronounced characteristic of those mixtures is their synergistic interactions, manifested from their low interfacial tension and low critical micelle concentration. By adjusting the composition, these interactions can be used to produce various assemblies from micelles to rod-like micelles or wormlike micelles and vesicles, which also result in abundant phase behavior such as a lyotropic liquid crystal and an aqueous surfactant two-phase system (ASTP) *etc.*[2–7] This situation has led to both theoretical and practical interest in investigating the phase behavior and physicochemical properties of mixed anionic and cationic surfactant systems.

The appearance of an ASTP has been a new visa for the isolation and purification of biomaterials and other compounds.[8–15] To fully utilize the advantages of the ASTP, the formation mechanism should first be understood. It is believed that the phase behavior of surfactant systems is closely related to the aggregates as well as the interaction between the aggregates. For example, Zhao *et al.*[16,17] found that an ASTP formed in a mixture of dodecyl triethyl ammonium bromide (C12NE) and sodium dodecyl sulfate (SDS) close to an equimolar ratio and attributed it to the coexistence of different micelles with distinct sizes. Our previous work studied whether the ASTP formed in dodecyl trimethyl ammonium (DTAB)–sodium laurate (SL) and related mixed systems.[18] The formation of an ASTP is attributed to the dense packing of vesicles and the formation of a lamellar structure in the surfactant-rich upper phase. Once the relationship between the microstructure and the phase behavior of surfactant systems is established, the ASTP formation can be modulated and optimized by changing environmental factors (such as concentration, composition, temperature, salt *etc.*) and varying the surfactant molecular structures, which effects the formation and transformation of the surfactant assemblies.[19–25]

Although there are some studies on the phase behavior of anionic and cationic mixed surfactant systems,[8–18,26–33] most of them are focused on conventional single-chain surfactants. Only a few reported works are concerned with Gemini surfactants.[29–33] As a novel type of surfactant, Gemini surfactants have attracted increasing attention over the past decades because of their many unusual physicochemical properties compared with conventional surfactants.[34,35] For a Gemini and conventional cationic surfactant mixed system, Shang *et al.*[29] and Nan *et al.*[30] investigated the phase behavior of a cationic Gemini surfactant 12-3-12 (ME)·2Br mixed with SDS or sodium dodecyl sulfonate.

[a]College of Petroleum Engineering, China University of Petroleum (East China), Qingdao 266580, Shandong Province, PR China. E-mail: HaimingFan@gmail.com; Fax: +86-532-86981701; Tel: +86-532-86983051

[b]Beijing National Laboratory for Molecular Sciences (BNLMS), State Key Laboratory for Structural Chemistry of Unstable and Stable Species, College of Chemistry, Peking University, Beijing 100871, PR China. E-mail: JBHuang@pku.edu.cn; Fax: +86-10-62751708; Tel: +86-10-62753557

They found that both systems showed only one Gemini-excess ASTP region in a very narrow range of molar ratio, which is different from conventional anionic and cationic surfactant mixed systems that usually have two ASTP regions. In our previous work, we investigated the effect of molecular structure on the ASTP formation by varying the polar head group size and the spacer length of cationic Gemini surfactants.[32] It was found that the area of the ASTP region for a mixture of C12–C6–C12 (Et)/SL is much larger than that of C12–C6–C12 (Me)/SL. Furthermore, an appropriate spacer length favors the formation of an ASTP. In this study, the phase behavior is investigated in the mixed system of an anionic Gemini surfactant, sodium dilauroyl cystine (SDLC), with a cationic surfactant, dodecyl trimethyl ammonium chloride (DTAC). It is found that the phase behavior undergoes changes from an isotropic homogeneous phase to an ASTP and then to an anisotropic homogeneous phase. The corresponding aggregate microstructures are investigated using rheology, dynamic light scattering, transmission electron microscopy (TEM) and polarization microscopy. The relationship between the phase behavior and the microstructures is established in order to understand the possible formation mechanism of an ASTP.

Experimental

Materials

The anionic Gemini surfactant, sodium dilauramino cystine (SDLC), is synthesized based on a procedure previously reported.[36,37] The cationic surfactant, dodecyl trimethyl ammonium chloride (DTAC, 99%), was purchased from the Alfa Aesar Company and recrystallized five times. The DTAC purity was examined and the surface tension minimum was found using the surface tension curve. Sudan III and borax are all A.R. grade and purchased from the Beijing Chemical Company. The water used was bi-distilled from potassium permanganate containing deionized water to remove traces of organic compounds. The pH values of the mixed systems were fixed at 9.2 using 10 mmol L^{-1} borax.

Sample preparation

Samples were prepared by mixing 15 mmol L^{-1} SDLC and the desired concentrations of DTAC in an aqueous buffer containing 10 mmol L^{-1} borax. After sealing, these samples were vortex-mixed and allowed to equilibrate in a 25 °C thermostatic bath for at least 72 h.

Rheology measurements

The rheological properties of the samples were measured with a Thermo Haake RS300 rheometer. A cone-plate sensor with a plate diameter of 35 mm and a cone angle of 2° was used. A chamber that covers the sample was used to avoid evaporation. The zero-shear viscosities were obtained in steady-state measurements, where a shear-rate sweep was performed in the range of 0.001–500 s^{-1}. Dynamic-state rheological measurements were performed at a constant shear stress of 0.2 Pa in the

linear viscoelastic region determined via dynamic stress sweep measurements. All measurements were performed at 25 °C.

Dynamic light scattering (DLS)

A spectrometer (ALV-5000/E/WIN Multiple Tau Digital Correlator) and a Spectra-Physics 2017 200 mW Ar laser operating at 514.5 nm were used to conduct the DLS. All solutions were filtered through a 0.45 μm hydrophilic PVDF membrane filter before the measurements. A photon correlation measurement, in the self-beating mode, was carried out at scattering angles of 30°–90°. The intensity autocorrelation functions were analyzed using the methods of CONTIN.[38] The apparent hydrodynamic radius, R_h, was deduced from the diffusion coefficient, D, using the Stokes–Einstein formula, $R_h = k_B T/(6\pi\eta D)$, where k_B is the Boltzmann constant, η is the solvent viscosity and T is the absolute temperature of the solution.

Transmission electron microscopy (TEM)

Micrographs were obtained with a JEM-100CX II transmission electron microscope using both the negative-staining method (with uranyl acetate) and the freeze-fracture replication technique. Fracturing and replication were carried out in an EE-FED.B freeze–fracture device equipped with a JEE-4X vacuum evaporator.

Polarization microscopy

Photographs of the birefringence sample were taken using an OLYMPUSBH-2 polarization microscope with Kodak-400 color film. The intensity of the incident light as well as the time of exposure remained constant.

Results and discussion

Phase behavior of the SDLC–DTAC mixed surfactant solutions

Photos of the 15 mmol L^{-1} SDLC–DTAC mixed surfactant solutions, with increasing concentration of DTAC, are given in Fig. 1. All of the samples from 15 mmol L^{-1} to 18 mmol L^{-1} are transparent viscoelastic isotropic homogeneous phases (Fig. 1a). By increasing the concentration of DTAC from 19 mmol L^{-1} to 20 mmol L^{-1}, the samples separate macroscopically into two phases (ASTP). The lower phases of the ASTP are
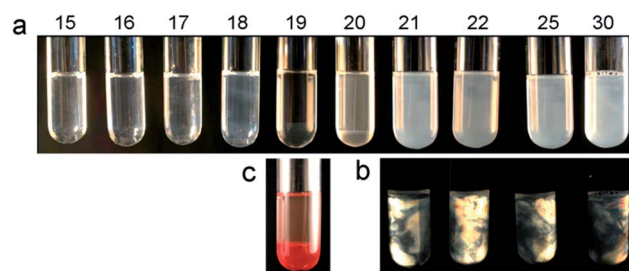
Fig. 1 Phase behavior of 15 mmol L^{-1} SDLC–DTAC mixed surfactant solutions (a) without crossed polarizer; (b) with crossed polarizer; (c) the ASTP upon the addition of Sudan III. The numbers above the photos are the DTAC concentrations (mmol L^{-1}).

viscoelastic isotropic solutions and the upper phases of the ASTP are clear solutions with a viscosity similar to water. For DTAC concentrations higher than 20 mmol L^{-1}, samples become opalescent single phases with birefringence (Fig. 1b). These opalescent solutions are stable for several weeks at 25 °C. The oil-soluble red dye Sudan III is added to show more details about the ASTP (Fig. 1c). It is clearly seen that the color of the lower phase is much darker than that of the upper phase, indicating that the lower one is the surfactant-rich phase, whereas the upper one is the surfactant-poor phase. A detailed measurement of the phase volume shows that the volume percentages of the upper and lower phases are extremely sensitive to the concentration of DTAC (Fig. 2). The volume percentage of the lower phase decreases, and accordingly the volume percentage of upper phase increases with an increase in the DTAC concentration.

Aggregate microstructures of the SDLC–DTAC mixed surfactant solutions

Usually, the macroscopic phase behavior is closely related to the microstructures in the surfactant systems. In order to further probe this relationship, the aggregate structures of the SDLC–DTAC mixed surfactant solutions are investigated. Fig. 3 shows the steady and dynamic rheological curves for the 15 mmol L^{-1} SDLC–17.5 mmol L^{-1} DTAC mixed solution. A Newtonian plateau at low shear rates followed by shear thinning at higher shear rates occurs in the steady shear viscosities (Fig. 3a), characterizing the formation of wormlike micelles.[39,40] This is because the elongated wormlike micelles become aligned in the shear flow direction when the shear rate is increased to a critical value as shown by Rheo-SANS experiments.[41] The degree of structural alignment correlates to the extent of shear thinning, which precedes a pronounced decrease in viscosity with increasing shear rate. The dynamic rheological properties of the wormlike micelles are shown in Fig. 3b. Clearly, the storage modulus (G') and the loss modulus (G'') have one crossover point. At frequencies below the crossover, the data points of G'
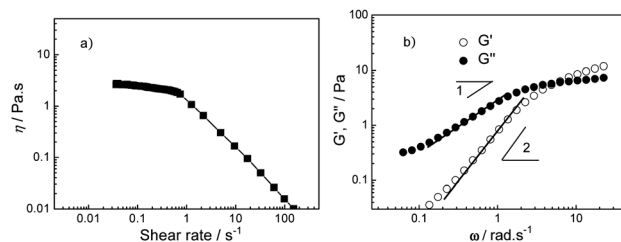
Fig. 3 Steady (a) and dynamic (b) rheological curves for the 15 mmol L^{-1} SDLC–17.5 mmol L^{-1} DTAC mixed solution. The lines in (b) fit eqn (1) and (2) of the Maxwell model.

and G'' are well fitted to the Maxwell model given by the following equations:[42]

$$G'(\omega) = \frac{G_0(\omega\tau_R)^2}{1 + (\omega\tau_R)^2} \tag{1}$$

$$G''(\omega) = \frac{G_0\omega\tau_R}{1 + (\omega\tau_R)^2} \tag{2}$$

where G_0 is the plateau modulus and τ_R is the relaxation time. Thus, in this region, G' and G'' increase with ω^2 and ω, respectively, which is also typical for wormlike micelles.

Fig. 4a shows the representative steady viscosities for the SDLC–DTAC mixed systems in the isotropic homogeneous phase region, which seems similar to the 15 mmol L^{-1} SDLC–17.5 mmol L^{-1} DTAC mixed solution and indicates the formation of wormlike micelles in these systems. In addition, the zero shear-viscosities (η_0, plateau viscosities) against the DTAC concentration exhibit a peak, suggesting that the wormlike micelles have a maximum contour length at a threshold DTAC concentration. It is well known that the micelles grow while staying linear up to the maximum concentration, whereas beyond the maximum, branching of the wormlike micelles occurs.[43–45] In the branched wormlike micelles, the inter-micellar junctions that can slide along the cylindrical body serve as stress-release points, so that the viscosity is reduced. Theoretical studies have predicted that branching of wormlike micelles should lower the viscosity, and so there is a foundation for this hypothesis. Recently, Croce et al.[46] observed the branching of wormlike micelles using cryo-TEM at a surfactant composition beyond the peak and Ziserman et al.[47] found that branching already occurs at the peak composition.
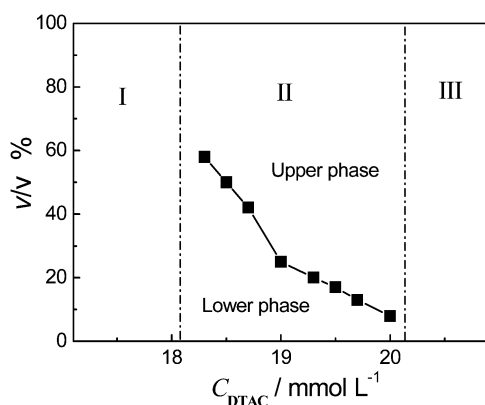
Fig. 2 Phase behavior features of 15 mmol L^{-1} SDLC–DTAC mixed solutions ((I), isotropic homogeneous phase; (II), ASTP, aqueous surfactant two-phase solutions; (III), anisotropic homogeneous phase).
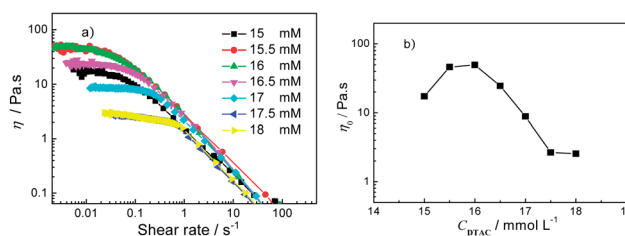
Fig. 4 Steady rheological curves (a) and the zero shear-viscosities, η_0, (b) with varying DTAC concentration in the isotropic homogeneous phase.

Nevertheless, from Fig. 4b it is seen that the wormlike micelles in the isotropic homogeneous phase region of the SDLC–DTAC mixed system are indeed formed and linear to branch growth.

In the ASTP region, the lower and upper phases are separated to determine the aggregate structures. Fig. 5 shows the steady and dynamic rheological curves for the ASTP lower phase of the 15 mmol L^{-1} SDLC–19 mmol L^{-1} DTAC mixed solution. It can be seen that the rheological responses are similar to Fig. 3 as discussed previously, which indicates wormlike micelles formed in the lower phase. It is worth noting that the G_0 and τ_R values of the present case are 348.9 Pa, 0.008 s and G_0 and τ_R values for the 15 mmol L^{-1} SDLC–17.5 mmol L^{-1} DTAC mixed solution are 8.1 Pa, 0.308 s. The higher G_0 and lower τ_R for the ASTP lower phase of the 15 mmol L^{-1} SDLC–19 mmol L^{-1} DTAC mixed solution compared to that of the 15 mmol L^{-1} SDLC–17.5 mmol L^{-1} DTAC mixed solution indicates that more branched wormlike micelles are formed in the former.[43–45]

The aggregate structure of the ASTP upper phase in the 15 mmol L^{-1} SDLC–19 mmol L^{-1} DTAC mixed solution is studied by dynamic light scattering (DLS) and transmission electron microscopy (TEM). The curves obtained from the CONTIN analysis of the DLS measurements at different scattering angles are shown in Fig. 6a, where a well-separated single distribution has been observed and does not show any angular dependence. By using the Stokes–Einstein equation, the corresponding apparent hydrodynamic radius ($\langle R_h \rangle$, peak of the R_h distribution curve) value was calculated to be 252 nm at a scattering angle of 90° and it represented the typical size of the aggregates. The TEM image demonstrated the existence of spherical vesicles with a diameter of 200–600 nm in this system (Fig. 6b). Combined with the fact that the apparent viscosity of the solution is nearly the same as water, the aggregates in the DLS plot should be assigned to vesicles. Thus, it can be concluded that vesicles exist in the ASTP upper phase of the 15 mmol L^{-1} SDLC–19 mmol L^{-1} DTAC mixed solution.

Further rheology and dynamic light scattering experiments are performed to investigate the aggregate microstructure changes in the ASTP region (Fig. 7). It can be seen that the plateau modulus, G_0, of the lower phases and apparent hydrodynamic radius, $\langle R_h \rangle$, of the upper phases increase with DTAC concentration. Firstly, G_0 obeys the following relationship:[48]

$$G_0 = \frac{k_B T}{\xi_M^{\,3}} \tag{3}$$
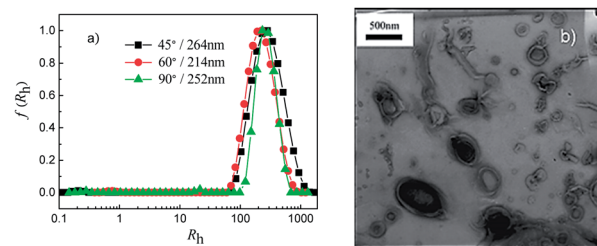
Fig. 6 Hydrodynamic radius R_h distribution (a) and a TEM image (b) for the ASTP upper phase of the 15 mmol L^{-1} SDLC–19 mmol L^{-1} DTAC mixed solution.

where ξ_M is the network mesh size of wormlike micelles. Therefore, the value of G_0 is in inversely proportionate to ξ_M and the increase in G_0 indicates that ξ_M decreases. Owing to the branched wormlike micelles formed in the lower phases, this may suggest that the branched extent of the wormlike micelles is gradually enhanced with the increase in DTAC concentration. Secondly, the increase in the $\langle R_h \rangle$ indicated that the vesicle sizes become larger. Therefore, the above experimental results reveal that the branched extent of the wormlike micelles is gradually enhanced in the lower phase and the vesicle sizes become larger and larger in the upper phase with the increase in DTAC concentration in the ASTP region.

For the anisotropic homogeneous phase, Fig. 8a shows the representative photographs under a polarization microscope. Colorful speckles formed by cross-like spherulite textures are observed. These textures demonstrate the existence of a lamellar liquid crystal phase,[18,49,50] which is corroborated by the FF-TEM image (Fig. 8b).

Mechanism of the microstructure and phase behavior transitions

It has been shown that during the continuous addition of DTAC to a 15 mmol L^{-1} SDLC aqueous solution from 15 mmol L^{-1} to 30 mmol L^{-1}, the phase behavior of the SDLC–DTAC cationic surfactant mixed systems transforms from an isotropic

Fig. 5 Steady (a) and dynamic (b) rheological curves for the ASTP lower phase of the 15 mmol L^{-1} SDLC–19 mmol L^{-1} DTAC mixed solution. The lines in (b) fit eqn (1) and (2) of the Maxwell model.
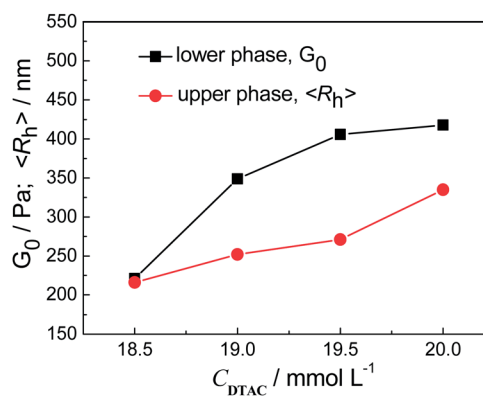
Fig. 7 The plateau modulus, G_0, of the lower phases and apparent hydrodynamic radius, $\langle R_h \rangle$, of the upper phases vary with the DTAC concentrations for the ASTP.
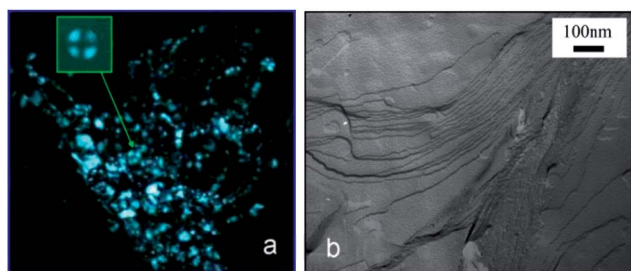
Fig. 8 Photograph through a polarization microscope (a) and a lamellar structure observed by FF-TEM (b) of the 15 mmol L^{-1} SDLC–30 mmol L^{-1} DTAC mixed solution.

homogeneous phase to an ASTP and then to an anisotropic homogeneous phase (Fig. 9). For the isotropic homogeneous phase, the aggregate microstructure is a wormlike micelle, which occurs linear to the branch growth with increasing DTAC concentration. In the ASTP region, the aggregate microstructures in the lower and upper phases are branched wormlike micelles and vesicles, respectively. The branched extent of the wormlike micelles was enhanced as indicated by the G_0 increasing from 221 Pa to 418 Pa and the apparent hydrodynamic radius of vesicles increasing from 216 nm to 335 nm with the increase in DTAC concentration. Furthermore, the volume percentage of the lower phase decreases by increasing the DTAC concentration, which indicates the branched wormlike micelle transformed into a vesicle. For the anisotropic homogeneous phase, the aggregate microstructure is a lamellar liquid crystal.

The mechanism of the aggregate microstructure transformation can be realized using the well-known theory of the packing parameter p, proposed by Israelachvili et al.[51,52] p is defined as v/a_0l_c, where v is the surfactant tail volume, l_c is the tail length and a_0 is the equilibrium area per molecule at the aggregate surface. This theory has been widely and successfully used to explain the transformations of aggregate microstructures in dilute surfactant solutions: $1/3 \leq p < 1/2$ for cylindrical micelles, $1/2 \leq p < 1$ for bilayer structures and $p = 1$ for planar extended bilayers. For the continuous additions of DTAC to a 15 mmol L^{-1} SDLC aqueous solution from 15 mmol L^{-1} to 30 mmol L^{-1}, the Gemini surfactant SDLC has two polar head groups, the anionic and cationic charge molar ratio in the mixed systems varies form 2 : 1 to 1 : 1. Thus, the electrostatic attraction between the anionic and cationic surfactant head group is strengthened by increasing the DTAC concentration, and then the equilibrium area per molecule a_0 decreases. It is conceivable that the variation of v and l_c will be insignificant for
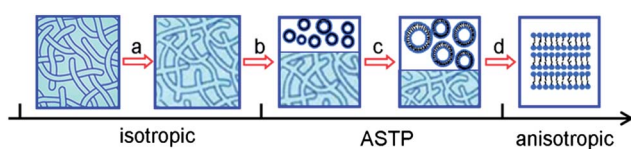
the SDLC–DTAC mixed system at different mixed molar ratios. Therefore, an increase in the aggregate parameter, p, can be expected, and the formation of larger aggregates with a low curvature is more favored. Hence, the aggregate microstructures undergo transitions from a wormlike micelle to vesicle and then to a lamellar structure.

The macroscopic phase behavior and microscopic aggregate structures are related to understanding the possible formation mechanisms for the ASTP. Phase separation occurs when the total attractive potential energy due to the attractive van der Waals forces and the repulsive electrostatic forces between components is greater than the thermal energy k_BT.[53–55] In the isotropic homogeneous region, adding DTAC decreases a_0, increases p and then promotes linear to branched growth of wormlike micelles. On the one hand, the surface charge density of the wormlike micelles decreases in this process, which leads to screening of the electrostatic repulsion between the SDLC–DTAC wormlike micelles. At the same time, the aggregate microstructure changes from linear to branched wormlike micelles, and a connected network of branched micelles will be more saturated than an entangled network of linear micelles. Consequently, the inter-aggregate distance gradually decreases as the wormlike micelle branching continues and strengthens the attractive van der Waals forces. The above influence factors produce a total attractive potential energy arising between the micelles, eventually promoting the tendency for phase separation and causing an ASTP to form in the SDLC–DTAC mixed surfactant system. In fact, previous theories suggest that, as branching proceeds, the system might eventually phase separate into a saturated micellar network with no free ends and a dilute surfactant solution.[56–58] Thus, wormlike micelle branching can provide a driving force for ASTP formation. However, our experimental results indicate that the branched wormlike micelle network varies and is far from a fully saturated state when the ASTP occurs, which is not completely coincident with the prediction of previous theories. It is found that vesicles form in the ASTP upper phase. The vesicle radius is more than 200 nm, whereas the mesh size of the branched wormlike micelles is less than 10 nm (calculated by eqn (3)), therefore the vesicles cannot exist in the network of branched wormlike micelles. These two distinct sizes and incompatible aggregates formed in the SDLC–DTAC mixed surfactant system further accelerate the occurrence of phase separation. Furthermore, it is worth noting that compared with the branched wormlike micelle, the surface charge of the vesicle is much closer to zero and they attract much fewer counter ions, which leads to a lower density. Therefore, the solution containing vesicles forms the upper phase of the ASTP. Combining the facts and analysis above, from the viewpoint of aggregate microstructure, synchronous formation of branched wormlike micelles and vesicles are the main driving forces of ASTP formation in our investigation.

Conclusions

In the present study, the phase behavior and aggregate microstructures are systematically studied in an anionic Gemini surfactant and a cationic conventional surfactant mixed system.

Fig. 9 Scheme of the phase behavior and aggregate microstructure transitions of the 15 mmol L^{-1} SDLC aqueous solution with the continuous addition of DTAC from 15 mmol L^{-1} to 30 mmol L^{-1}.

It is demonstrated that the phase behavior undergoes changes from an isotropic homogeneous phase to an ASTP and then to an anisotropic homogeneous phase, which is closely related to the aggregate microstructures and their interactions. Isotropic or anisotropic homogeneous phases were formed of a single aggregate, namely a wormlike micelle or a lamellar structure, whereas the formation of an ASTP can be attributed to the coexistence of branched wormlike micelles and vesicles. Wormlike micelle branching might enhance the total attractive potential energy between the aggregates by decreasing the surface charge density and inter-aggregate interaction distance and provide a driving force for ASTP formation. Two distinct sizes and incompatible aggregates composed of vesicles and branched wormlike micelles also accelerate the occurrence of the phase separation. From the mixed Gemini surfactant and oppositely charged conventional surfactant system, our studies may provide further understanding of the relationship between the macroscopic phase behavior and microscopic aggregate structures, which may also advance the ASTP applications in correlative fields.

Acknowledgements

Notes and references

1 *Mixed Surfactant Systems*, ACS Symposium Series 501, ed. P. M. Holland and D. N. Rubingh, American Chemical Society, Washington DC, 1992.

2 E. W. Kaler, A. K. Murthy, B. E. Rodriguez and J. A. Zasadzinski, *Science*, 1989, **245**, 1371–1374.

3 H. Rehage and H. Hoffmann, *J. Phys. Chem.*, 1988, **92**, 4712–4719.

4 X. F. Li and H. Kunieda, *Langmuir*, 2000, **16**, 10092–10100.

5 S. R. Raghavan, H. Edlund and E. W. Kaler, *Langmuir*, 2002, **18**, 1056–1064.

6 M. Mao, J. B. Huang, B. Y. Zhu and J. P. Ye, *J. Phys. Chem. B*, 2002, **106**, 219–225.

7 Y. Q. Nan, H. L. Liu and Y. Hu, *Colloids Surf., A*, 2005, **269**, 101–111.

8 O. Bermudez and D. Forciniti, *Biotechnol. Prog.*, 2004, **20**, 289–298.

9 M. S. Long and C. D. Keating, *Anal. Chem.*, 2006, **78**, 379–386.

10 C. L. Liu, D. T. Kamei, J. A. King, D. I. C. Wang and D. Blankschtein, *J. Chromatogr., Biomed. Appl.*, 1998, **711**, 127–138.

11 Y. Akama, A. J. Tong, M. Ito and S. Tanaka, *Talanta*, 1999, **48**, 1133–1137.

12 A. J. Tong, J. J. Dong and L. D. Li, *Anal. Chim. Acta*, 1999, **390**, 125–131.

13 J. X. Xiao, U. Sivars and F. J. Tjerneld, *J. Chromatogr., Biomed. Appl.*, 2000, **743**, 327–338.

14 Y. Akama, M. Ito and S. Tanaka, *Talanta*, 2000, **53**, 645–650.

15 Y. Akama and A. Sali, *Talanta*, 2000, **57**, 681–686.

16 Z. J. Yu and G. X. Zhao, *J. Colloid Interface Sci.*, 1989, **130**, 421–431.

17 G. X. Zhao and J. X. Xiao, *J. Colloid Interface Sci.*, 1996, **177**, 513–518.

18 H. Q. Yin, M. Mao, J. B. Huang and H. L. Fu, *Langmuir*, 2002, **18**, 9198–9203.

19 R. Beck, Y. Abe, T. Terabayashi and H. Hoffmann, *J. Phys. Chem. B*, 2002, **106**, 3335–3338.

20 J. C. Hao, J. Z. Wang, W. M. Liu, R. Abdel-Rahem and H. Hoffmann, *J. Phys. Chem. B*, 2004, **108**, 1168–1172.

21 P. A. Hassan, S. R. Raghavan and E. W. Kaler, *Langmuir*, 2002, **18**, 2543–2548.

22 M. Johnsson, A. Wagenaar and J. B. F. N. Engberts, *J. Am. Chem. Soc.*, 2003, **125**, 757–760.

23 Y. Yan, W. Xiong, X. S. Li, T. Lu, J. B. Huang, Z. C. Li and H. L. Fu, *J. Phys. Chem. B*, 2007, **111**, 2225–2230.

24 P. R. Majhi and A. Blume, *J. Phys. Chem. B*, 2002, **106**, 10753–10763.

25 H. Q. Yin, Z. K. Zhou, J. B. Huang, R. Zheng and Y. Y. Zhang, *Angew. Chem., Int. Ed.*, 2003, **42**, 2188–2191.

26 M. T. Yatcilla, K. L. Herrington, L. L. Brasher, E. W. Kaler, S. Chirurolu and J. A. Zasadzinski, *J. Phys. Chem.*, 1996, **100**, 5874–5879.

27 X. H. Wang, X. L. Wei, J. Liu, J. F. Liu, D. Z. Sun, P. P. Du and A. L. Ping, *Fluid Phase Equilib.*, 2013, **347**, 1–7.

28 K. Wang, H. Q. Yin, J. B. Huang, W. Sha and H. L. Fu, *J. Phys. Chem. B*, 2007, **111**, 12997–13005.

29 Y. Z. Shang, H. L. Liu, Y. Hu and J. M. Prausnitz, *Colloids Surf., A*, 2007, **302**, 58–66.

30 Y. Q. Nan, H. L. Liu and Y. Hu, *J. Colloid Interface Sci.*, 2006, **293**, 464–474.

31 R. Jiang, Y. X. Huang, J. X. Zhao and C. C. Huang, *Fluid Phase Equilib.*, 2009, **277**, 114–120.

32 T. Lu, Z. H. Li, J. B. Huang and H. L. Fu, *Langmuir*, 2008, **24**, 10723–10728.

33 Y. Zhao, Y. Yan, L. X. Jiang, J. B. Huang and H. Hoffmann, *Soft Matter*, 2009, **5**, 4250–4255.

34 F. M. Menger and J. S. Keiper, *Angew. Chem., Int. Ed.*, 2000, **39**, 1906–1920.

35 R. Zana, *Adv. Colloid Interface Sci.*, 2002, **97**, 203–220.

36 H. M. Fan, F. Han, Z. Liu, L. Qin, Z. C. Li, D. L. Liang, F. Y. Ke, J. B. Huang and H. L. Fu, *J. Colloid Interface Sci.*, 2008, **321**, 227–234.

37 H. M. Fan, L. W. Meng, Y. J. Wang, X. Y. Wu, S. R. Liu, Y. Li and W. L. Kang, *Colloids Surf., A*, 2011, **384**, 194–199.

38 S. W. Provencher, *Comput. Phys. Commun.*, 1982, **27**, 213–227.

39 M. E. Cates and S. J. Candau, *J. Phys.: Condens. Matter*, 1990, **2**, 6869–6892.

40 H. Rehage and H. Hoffmann, *Mol. Phys.*, 1991, **74**, 933–973.

41 S. Förster, E. Wenz and P. Lindner, *Phys. Rev. Lett.*, 2005, **94**, 017803.

42 P. Koshy, V. K. Aswal, M. Venkatesh and P. A. Hassan, *J. Phys. Chem. B*, 2011, **115**, 10817–10825.

43 R. Oda, P. Panizza, M. Schmutz and F. Lequeux, *Langmuir*, 1997, **13**, 6407–6412.

44 A. Bernheim-Groswasser, T. Tlusty, S. A. Safran and Y. Talmon, *Langmuir*, 1995, **15**, 5448–5453.

45 H. M. Fan, Y. Yan, Z. C. Li, Y. Xu, L. X. Jiang, L. M. Xu, B. Zhang and J. B. Huang, *J. Colloid Interface Sci.*, 2010, **348**, 491–497.

46 V. Croce, T. Cosgrove, G. Maitland, T. Hughes and G. Karlsson, *Langmuir*, 2003, **19**, 8536–8541.

47 L. Ziserman, L. Abezgauz, O. Ramon, S. R. Raghavan and D. Danino, *Langmuir*, 2009, **25**, 10483–10489.

48 M. Doi and S. F. Edwards, *The Theory of Polymer Dynamic*, Clarendon, Oxford, UK, 1986.

49 Y. W. Shen, H. Hoffmann and J. C. Hao, *Langmuir*, 2009, **25**, 10540–10547.

50 J. Zhang, A. X. Song, Z. B. Li, G. Y. Xu and J. C. Hao, *J. Phys. Chem. B*, 2000, **114**, 13128–13135.

51 J. N. Israelachvili, D. J. Mitchell and B. W. Ninham, *J. Chem. Soc., Faraday Trans. 2*, 1976, **72**, 1525–1567.

52 J. N. Israelachvili, D. J. Mitchell and B. W. Ninham, *Biochim. Biophys. Acta, Biomembr.*, 1977, **470**, 185–201.

53 J. D. Gunton, M. San Miguel and P. S. Sahni, *Phase transitions and critical phenomena*, Academic, London, 1983, vol. 8.

54 T. Cosgrove, *Colloid Science: Principles, Methods and Applications*, Blackwell Publishing, Oxford, UK, 2005.

55 J. Lyklema, H. P. van Leeuwen and M. Minor, *Adv. Colloid Interface Sci.*, 1999, **83**, 33–69.

56 T. J. Drye and M. E. Cates, *J. Chem. Phys.*, 1992, **96**, 1367–1375.

57 P. Panizza, G. Cristobal and J. Curely, *J. Phys.: Condens. Matter*, 1998, **10**, 11659–11678.

58 G. Cristobal, J. Rouch, J. Curely and P. Panizza, *Phys. A*, 1999, **268**, 50–64.